NashFormer: Leveraging Local Nash Equilibria for Semantically Diverse Trajectory Prediction

Justin Lidard^{1,3}, Oswin So², Yanxia Zhang³, Jonathan DeCastro³, Xiongyi Cui³, Xin Huang² Yen-Ling Kuo², John Leonard³, Avinash Balachandran³, Naomi Ehrich Leonard¹ and Guy Rosman³

Abstract-Interactions between road agents present a significant challenge in trajectory prediction, especially in cases involving multiple agents. Because existing diversity-aware predictors do not account for the interactive nature of multiagent predictions, they may miss these important interaction outcomes. In this paper, we propose NashFormer, a framework for trajectory prediction that leverages game-theoretic inverse reinforcement learning to improve coverage of multi-modal predictions. We use a training-time game-theoretic analysis as an auxiliary loss resulting in improved coverage and accuracy without presuming a taxonomy of actions for the agents. We demonstrate our approach on the interactive split of the Waymo Open Motion Dataset, including four subsets involving scenarios with high interaction complexity. Experiment results show that our predictor produces accurate predictions while covering 33% more potential interactions versus a baseline model.

I. INTRODUCTION

Motion forecasting is a critical task in autonomous driving for understanding distinct interactive behaviors of road agents and making safe decisions. In *joint* motion prediction, which involves predicting trajectories for multiple agents simultaneously, the problem of covering many possible outcomes is exacerbated by the existence of many feasible modes of interaction, especially in dense or urban environments. Many recent works employ inference-time sampling techniques [1]–[5] produce a set of representative samples from a much larger proposal distribution, from which diversity can be evaluated post-hoc.

On the other hand, some recent works promote sample diversity instead by affording exploration in the space of discrete semantic representations, typically waypoints [2, 6] or maneuvers [7, 8]. However, an explicit latent representation could limit predictive diversity: predicted waypoints may be highly dependent on the type of interaction mode, and predicted maneuvers are limited to a *taxonomy* of handlabeled behaviors, which may be difficult and time-consuming to produce.

There remain several open challenges in multi-modal prediction methods in learning meaningful semantic behaviors without cumbersome hand-labeling, and in creating sampling techniques where sample diversity is evaluated and optimized

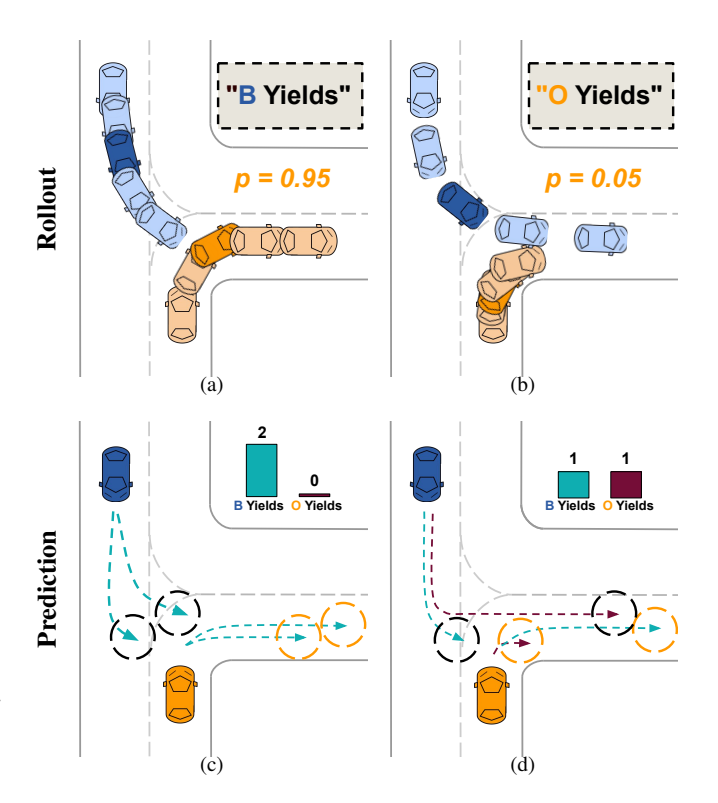


Fig. 1: An illustrative example where agents O and B navigate an intersection with different semantic interaction modes: (a) with higher probability (p=0.95), B yields to O with both agents respecting right-of-way, and (b) with lower probability (p=0.05), O yields to B after B ignores oncoming O, inconveniencing O. We show two prediction strategies with limited samples (K=2) (c) a generic predictor uses a metric sampling method such as non-maximum suppression [2] (dashed circles) and produces two likely but similar trajectories (both teal), and (d) our method captures payoff diversity and finds both distinct outcomes (teal, maroon) without predicting the semantic label.

at inference time. Our insight is to use game-theoretic techniques both for evaluating semantically distinct behaviors and for sampling optimally diverse trajectories, without explicitly labeling distinct outcomes with a manually defined taxonomy.

Fig. 1 illustrates a simple motivating example wherein existing predictors may fail to capture interactions of interest (failing to yield, Fig. 1b). The distinct outcomes of such interactions, while intuitive for human drivers, are not captured via the generic predictor (Fig. 1c), which uses a sampling

¹Department of Mechanical and Aerospace Engineering, Princeton University, Princeton, NJ 08540, USA, jlidard@princeton.edu

²Massachusetts Institute of Technology, Cambridge, MA 02139, USA

³Toyota Research Institute, Cambridge, MA 02139, USA

This research has been supported in part by an NSF Graduate Research Fellowship. This article solely reflects the opinions and conclusions of its authors and not TRI or any other Toyota entity.

method such as NMS to find metrically distinct trajectories, but falls short of finding the other semantic mode where the orange agent yields. A game-aware predictor such as NashFormer will capture both semantic scenarios.

In this paper, we develop and implement NashFormer: a methodology that leverages the fundamental idea that segmentation of a candidate trajectory predictions according to nearby local Nash equilibria (LNEs) promotes *tunable* diversity at training time, and permits *inference-time* diverse sampling. We design a method for covering equilibria that are diverse in terms of learned utility and show that our method provides *semantic* diversity, without requiring hand-labeled semantic features.

Our main contributions are as follows:

- A prediction model that covers semantically distinct LNE,
- A game-theoretic analysis module for evaluating, scoring and clustering candidate candidate trajectories,
- Experimental results on the Waymo interactive dataset, including strongly interactive subsets of the dataset.
 These demonstrate the accuracy and coverage of our predictions and provide insight into the influence of model parameters.

II. RELATED WORK

Our work relates to several topics in game-theoretic planning and joint trajectory prediction.

A. Dynamic Games and Inverse Optimal Control

Dynamic games [9] are a common framework for analyzing N-player driving scenarios [10]–[13]. Optimal control policies satisfy Local Nash Equilibrium (LNE), where each player's expected payoff is locally optimal with respect to their control strategy. LNEs have been studied extensively in autonomous driving as a model for interaction in merging [14, 15], highway overtaking [10, 16], and racing [12, 17]. Recent works in game-theoretic planning give efficient methods for solving LNE for deterministic policies [15] and stochastic policies (i.e. bounded rationality) [18]. Extensions have also been presented to games where agent's actions are determined under partial state observations [17] or by some latent parameters in the policy [19, 20] or cost [16]. Some recent works [13, 21] have addressed multi-modal planning under a discrete latent variable, but providing efficient and context-dependent methods for trajectory prediction under many possible modes of interaction is an open challenge.

Inverse optimal control and reward learning have been used, even at the single agent level, for understanding human decision-making [22]–[25], facilitating analysis of *bounded rational* decision making for road agents under a maximum entropy (MaxEnt), non-greedy framework. The reward-learning approach most similar to ours in spirit is that of [14]. In [14], the parameters of a quadratic potential game are learned, and then the optimal policies of each agent are solved online to predict the outcome of a highway merge scenario between two agents. Our work is different in three ways: (i) we permit stochastic (bounded-rational) learned policies under

beyond maximum-entropy framework, (ii) we leverage inverse reinforcement learning (IRL) to learn LNE during training and efficient evaluate coverage during inference time (iii) we evaluate our framework on real driving scenarios of varying complexity.

B. Multi-agent Prediction

Within the field of trajectory prediction, agent-agent interactions are a critical consideration when scaling to the multi-agent setting [26]. The output of a joint predictor may be a raw trajectory sample [6], a weighted set [27], or a mixture model over discrete modes [28]. Finally, some approaches explicitly model discrete agent interactions in order to better account for them and improve accuracy [29]–[31]. Our work, however, specifically emphasizes *multi-modality* and offline rollouts to replace fictitious play in the prediction framework.

C. Diverse Prediction

In sample-based prediction, maintaining diversity of samples to represent distinct outcomes is an active area of research. Farthest Point Sampling (FPS) [7, 32], Non-Maximum Suppression (NMS) [2], and/or neural adaptive sampling [8] provide methods for encouraging outcome diversity using pairwise distances between trajectories as a metric. Diversity in the sampling is often aided by specific underlying representation, such as a latent layer in [33], a mixture model [34], a set of anchor points [3], or the use of a bagging algorithm on the trajectories [35]. Several works [36, 37] show that knowledge of downstream tasks allows adaptation of the prediction samples so as to improve results. In our paper we show that with learned game-theoretic utilities, our prediction framework achieves better coverage of semantic interactions without the need for explicit taxonomies or task definition for semantic coverage.

III. APPROACH

This section details our procedure for approximating the LNE of the system by modeling it as an inverse maximum-entropy dynamic game. Using the approximated LNE, we segment candidate trajectories according to their nearest LNE and compute a (differentiable) empirical histogram that represents of the relative coverage of each LNE across the full sample set. The empirical histogram is compared via the Kullback-Liebler (KL) divergence to a tunable "ideal" histogram determined by the game-theoretic likelihood of the LNE. The KL-divergence score functions as an auxiliary coverage loss during training. At inference time, the empirical histogram may be used to mask duplicate interactive behaviors in a proceedure similar to non-maximum supression (NMS).

A. Inverse Maximum-Entropy Dynamic Games

In order to characterize the LNEs in each scenario, we first approximate road agents behavior as a discrete dynamic game. The joint state of the dynamic game follows a nonlinear dynamics equation:

$$\mathbf{x}_{t+1} = f_t(\mathbf{x}_t, u_t^1, u_t^2, ..., u_t^I) \quad \forall t$$
 (1)

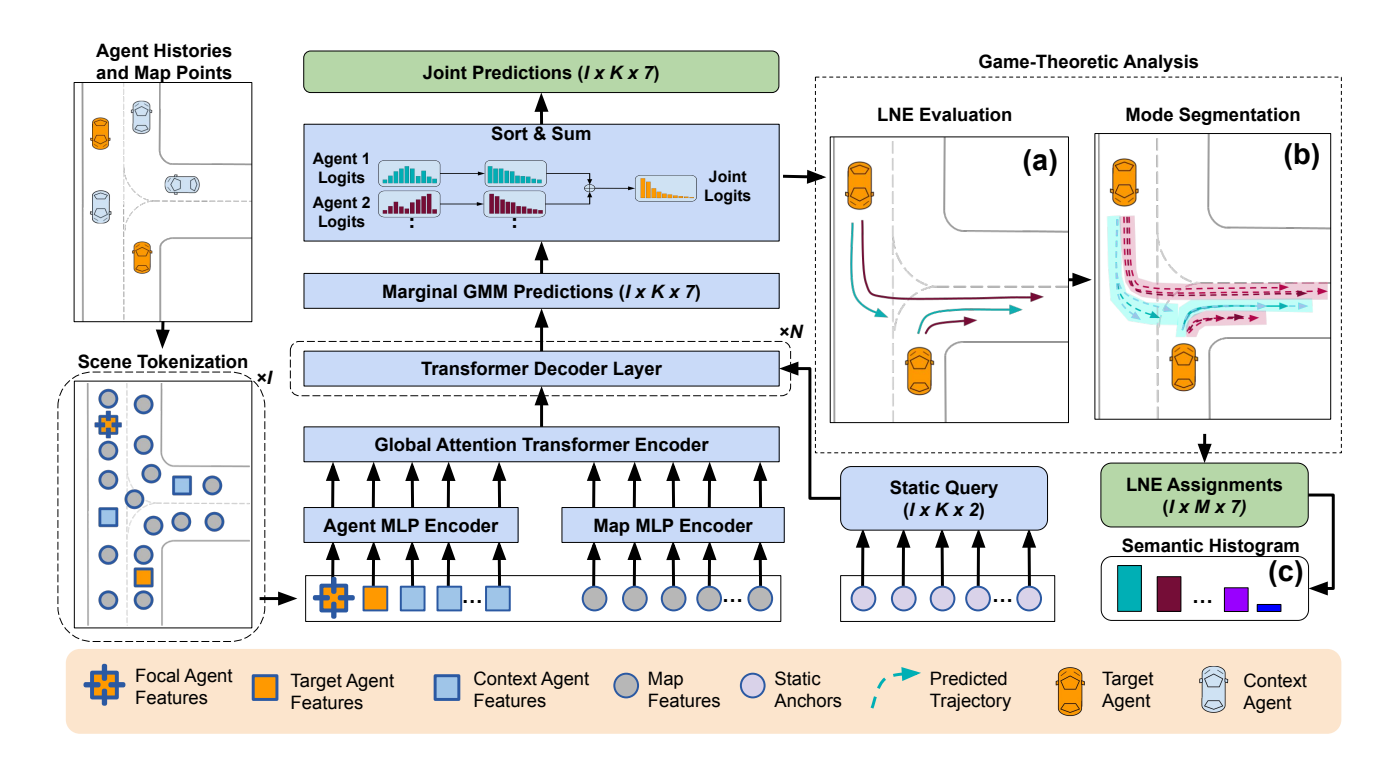


Fig. 2: Prediction system training architecture. Multi-agent trajectories and map polylines are tokenized in the local coordinates of each focal agent (blue outline) in the target agent set (orange) and processed in parallel using a network with shared weights. The encoded features are cross-attended using a transformer encoder. N transformer decoder layers refine the K candidate modes, and game-theoretic analysis scores the semantically meaningful modes: (a) candidate trajectories are optimized for their utility to find LNE, (b) modes are clustered according to the nearest LNE, and (c) the assigned modes are summarized in a semantic histogram. The final transformer decoder layer produces the final prediction for post-processing.

where $\mathbf{x}_t = (x_t^1, ..., x_t^I)$ denotes the joint state of the system and I is the number of decision-making agents. Under eqn. (1), agents affect the joint system simultaneously and non-cooperatively, and we model equilibria as Nash.

NashFormer learns the agent-level best-response model that evaluates the utility of an action u_t^i by agent i conditioned on the joint state \mathbf{x}_t , contrasting other direct-solving methods [11, 15] which may have poor coverage of equilibria. The model computes the log-likelihood actions for each agent i, based on a maximum entropy objective:

$$J^{i}(\pi^{i}) = \mathbb{E}^{\pi} \left[\sum_{t=1}^{T} r^{i}(\mathbf{x}_{t}, \mathbf{u}_{t}) + H[\pi^{i}(\cdot|\mathbf{x}_{t})] \right], \qquad (2)$$

where $\sum_{t=1}^{T} r^i(\mathbf{x}_t, \mathbf{u}_t)$ is the cumulative reward attained by agent i over the joint trajectory $\boldsymbol{\tau}$ and $H[\pi^i(\cdot|\mathbf{x}_t)]$ is the Shannon entropy of agent i's policy. We learn the policy π^i for each agent i that maximizes the objective in eqn. (2).

Several works [13, 38, 39] show that the LNE policies satisfy the coupled Boltzmann distributions:

$$\pi^{i}(u|\mathbf{x}) = \exp\left(A^{i}(\mathbf{x}, u)\right) \quad \forall \pi^{i}$$
 (3)

where A^i is the advantage function

$$A^{i}(\mathbf{x}, u) = \bar{Q}^{i}(\mathbf{x}, u) - V^{i}(\mathbf{x}), \tag{4}$$

with $\bar{Q}^i(\mathbf{x}_t, u_t^i)$ defined as an expectation over the policies of all other agents $\neg i$, as given by

$$\bar{Q}^{i}(\mathbf{x}, u) := \mathbb{E}^{\pi^{\neg i}}[Q^{i}(\mathbf{x}, \mathbf{u})], \tag{5}$$

Eqn. (5) reflects the *best response* of agent i to the expected actions of all other agents $\neg i$. As a consequence, the policy of agent i given in eqns. (3) and (5) is a function only of the payoffs of the actions of agent i. Next, we detail a learning procedure for eqn. (5).

Given a dataset \mathcal{D} of state-action histories of each agent (i.e., *trajectories*), we regress a log-likelihood of a single agent's action, conditioned on the multi-agent history, as given by Eqn. (3). We assume all agents in the data follow LNE and compute the best response in Eqn. (5) so as to avoid the inner expectation in Eqn. (3). We maximize the log-probability of individual state-action pairs, which is equivalent to maximizing the advantage function:

$$\log \pi^i(u|\mathbf{x}) = A^i(\mathbf{x}, u). \tag{6}$$

Using the item loss (6), we seek to learn the multi-agent MaxEnt policy that maximizes the likelihood of the data:

$$\mathcal{L}_{IRL}(\mathcal{D}) = -\mathbb{E}^{\boldsymbol{\tau} \sim \mathcal{D}} \left[\frac{1}{TA} \sum_{t=1}^{T} \sum_{i=1}^{A} \log \pi^{i} (u_{t}^{i} | \mathbf{x}_{t}) \right]. \quad (7)$$

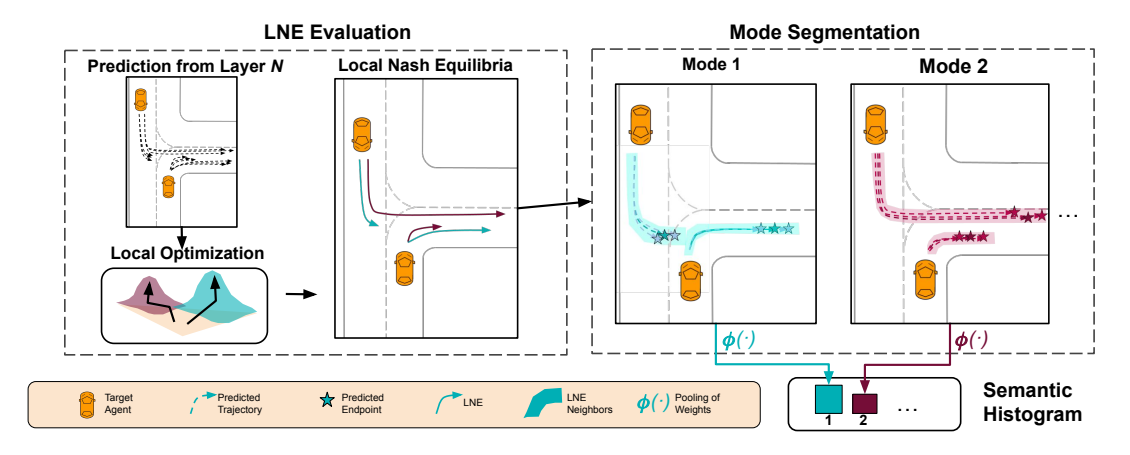


Fig. 3: Mode optimization module. The prediction from the final transformer decoder layer is given as input to a local optimization algorithm [40] to find the LNE. The closest LNE to each prediction are labeled, and the prediction weight belonging to each LNE are summed and normalized to create a histogram.

B. Enumerating Local Nash Equilibria

In this section, we detail how representative LNE are distilled in Fig. 2(a-c). By iteratively evaluating (3), the log-likelihood of a joint trajectory $\tau := (\tau^1, ..., \tau^I) = ((\mathbf{x}_1, \mathbf{u}_1), (\mathbf{x}_2, \mathbf{u}_2), ..., (\mathbf{x}_t, \mathbf{u}_T))$ is given as

$$\log p(\boldsymbol{\tau}) = \sum_{t=1}^{T} \sum_{i=1}^{I} \log \pi^{i}(u_{t}^{i}|\mathbf{x}_{t}). \tag{8}$$

under deterministic dynamics. Hence, each mode of $p(\tau)$ (locally) maximizes the *cumulative advantage*

$$A(\tau) := \sum_{t=1}^{T} \sum_{i=1}^{I} A^{i}(\mathbf{x}_{t}, u_{t}), \tag{9}$$

i.e. the sum of the utilities of each agent along a joint trajectory. In the next sections, we detail how the representative LNE and their weights are computed using the Mean Shift algorithm (LNE Evaluation), how candidate trajectories are assigned to the "nearest" LNE (Mode Segmentation), and finally how the segmented modes are summarized in a histogram according to their weights (semantic histogram).

a) LNE Evaluation: We employ the Mean Shift [40,41] algorithm to explore the game-theoretic modes of the posterior distribution over trajectories, in terms of their sum of utility along the trajectory. The LNE evaluation module takes as input a set S of L multi-agent trajectories emitted from the predictor. We evaluate the maximum-entropy likelihood of multi-agent trajectories, and iteratively seek distinct modes. To explore candidate trajectories, we utilize the dense outputs of the first N transformer decoder layers, consisting of L samples. Each output k is scored using (9) to compute $A(\tau_k)$. The set of sampled scores $\{A(\tau_k)\}_{k=1}^L$ is given as input to the Mean Shift optimizer and evaluated using their Boltzmann weights to compute the following kernel:

$$p(\boldsymbol{\tau}, \boldsymbol{\tau}') = \exp(A(\boldsymbol{\tau}) - A(\boldsymbol{\tau}')) \mathbb{1}\{d(\boldsymbol{\tau}, \boldsymbol{\tau}') < b\}). \tag{10}$$

Intuitively, the first term in eqn (10) promotes modes that have a higher advantage (evaluated over a full trajectory) than other nearby modes. The second term in (10) nullifies trajectories are far away in norm, d is the average (over agents) Euclidean distance between trajectory endpoints, and b is a tunable bandwidth.

b) Mode Segmentation: The output of the Mean Shift algorithm gives a set of $M \leq K$ locally optimal multiagent trajectories and their weights $\{A(\tau_k)\}_{k=1}^L$. From this set, we compute a set of labels \boldsymbol{L} that assigns each prediction from the final decoder layer to the nearest LNE, using the nearest-neighbor algorithm. Each element \boldsymbol{L}_k gives a one-hot embedding in $\{0,1\}^M$.

c) Semantic Histogram: The representative modes are used to compute a differentiable histogram. Given the LNE labels L, and mode weights $\{A^k(\tau)\}_{k=1}^L$, the density corresponding to each LNE is computed as

$$q_m^*(\boldsymbol{\tau}; \rho) = S\left(\rho \cdot \phi(A(\boldsymbol{\tau}_m^1), ..., A(\boldsymbol{\tau}_m^{N_m}))\right)$$
(11)

where N_m is the number of trajectories with label m, $\{\boldsymbol{\tau}_m^k\}_{k=1}^{N_m}$ are the segmented trajectories closest to mode m, $\phi(\cdot)$ denotes max-pooling, a $S(\cdot)$ denotes the softmax operation, and ρ is a shape parameter. We refer to this histogram as the *Boltzmann weights* of the representative LNE. We show later in this section how eqn. (11) is used in the computation of a training-time auxiliary loss to promote sample diversity, wherein higher-entropy semantic histograms indicate uniform coverage of each semantic mode found by Mean Shift, and hence sample diversity.

C. Model Details

a) Input Representation: Let N be the number of agents in the scene for the scene and I be the number of target agents, for whom we make a prediction. For each focal agent $i \in [I]$, the transformer encodes the state and map information in the coordinate frame aligned with the heading angle of agent i.

The state history is input as $X^i \in \mathbb{R}^{N \times T_0 \times C_k}$, where T_0 is the past horizon and C_k is the coordinate dimension of the state histories that includes kinematic information, including position, velocity, acceleration, yaw, and yaw rate in agent-local coordinates. The map is input as $M^i \in \mathbb{R}^{N_s \times N_p \times C_m}$, where N_s is the number of map segments, N_p is the number of points per segment, and C_m is the coordinate dimension of the map that includes the position, normal vector, and tangent vector of each map segment. Each agent's originally consists of N_m points, which we then arrange into N_s segments of at most N_p points consisting of its nearest neighbors. We zero-pad segments of less than N_p points.

- b) Encoder and Decoder Structure: Agent and map features are computed, in the local coordinates of each target agent $i \in [I]$ and in parallel. As shown in Fig. 2, the agent and map encoders takes as input the observed agent features and map segments about the scene over a fixed past horizon T_0 in agent local coordinates. The encoder and decoder structure are identical to [3].
- c) Sample Selection: In trajectory prediction, the number of trajectory samples is limited, typically to S=6. To increase the intrinsic diversity of samples we explore several post processing techniques: FPS, NMS, and a novel technique that suppresses non-LNE. FPS [1] iteratively maximizes the l_2 -distance between samples. The NMS procedure [2] takes as input a set of weighted samples, and iteratively constructs a set of representative samples by taking the highest-weighted samples within a ball of a pre-defined radius.

To encourage sampling of diverse interactive behaviors in the online setting, we introduce a new sampling method, *Non-Equilibrium Suppression* (NES), which functions similarly to NMS but uses the LNE assignments \boldsymbol{L} defined in section III.B to suppress samples with the same mode assignment until all LNE have been sampled.

D. Loss Definitions

We train NashFormer by jointly optimizing prediction accuracy, prediction classification, and mode coverage.

a) Prediction Loss: In line with other multimodal prediction literature that use weighted trajectory sets [3, 27, 28], we chose for each agent a multi-agent Gaussian mixture model with K components that represents the marginal likelihood of an observed point $o_t^i = (x_t^i, y_t^i)$:

$$P^{i}(o_{t}^{i}) = \sum_{k=1}^{K} p_{k,t}^{i} f_{k,t}^{i} (x_{t}^{i} - \mu_{x,t}^{i}, y_{t}^{i} - \mu_{y,t}^{i})$$
 (12)

where $f_{k,t}^i(\cdot,\cdot)$ is the component (Guassian) likelihood of the *i*th agent's observation o_t^i , and $p_{k,t}^i$ is the occurrence probability of the *i*th agent's motion mode.

The accuracy loss is given as the mean cumulative log-likelihood of the closest component h^i for each agent i over the time horizon T, i.e.

$$\mathcal{L}_{acc} = -\frac{1}{A} \sum_{i=1}^{A} \sum_{t=1}^{T} \left(\log p_{k,t}^{i} + \log f_{k,t}^{i} (x_{t}^{i} - \mu_{x,t}^{i}, y_{t}^{i} - \mu_{y,t}^{i}) \right). \tag{13}$$

We choose the index where the average ground truth distance of each agent's endpoints to the motion mode endpoints are minimized.

b) Classification Loss: As in [3,27,28], we learn a weight distribution w that describes the marginal likelihood of each motion mode. The marginal likelihoods are learned via a cross entropy loss

$$\mathcal{L}_{class} = -\sum_{k=1}^{K} \mathbb{1}\{k = \hat{k}\} \log w_k,$$
 (14)

which penalizes trajectories that are weighted highly but classified as different motion modes. The marginal log-probabilities are then sorted and summed to get the joint trajectory likelihood, i.e. the full summation in (7). We also use an l_1 velocity loss and a dense prediction loss as in [3].

c) Coverage Loss: To ensure maximal representation of the learned LNE in the final samples, we propose a novel coverage loss \mathcal{L}_{cov} , given as the KL-divergence between discrete semantic histogram (11) and the histogram obtained from the emitted trajectory set \mathcal{S} , described next. Similar to (11), we approximate a discrete distribution q_m over the mode support [1, ..., M], given as the softmax operation

$$q_m(\mathcal{S}) = S\left(\sum_{k=1}^K A(\boldsymbol{\tau}_k) \mathbb{1}\{\boldsymbol{L}_k = m\}\right)$$
(15)

For each mode m, (15) sums the contribution of each sample to the empirical mode likelihood.

The predicted mode distribution in (15) is contrasted with the mode distribution according to the game-theoretic (Boltzmann) model, which is approximated discretely as eqn. (11). where $\rho \to 0$ results in a uniform distribution for q^* over the top M game-theoretic modes). The predictor's coverage loss thus defined as the KL-divergence between q and q^* , i.e.

$$\mathcal{L}_{cov} = D_{KL}[q \mid | q^*]. \tag{16}$$

d) Final Loss: The final loss is computed as

$$\mathcal{L} = \alpha \mathcal{L}_{acc} + \beta \mathcal{L}_{class} + \gamma \mathcal{L}_{cov}. \tag{17}$$

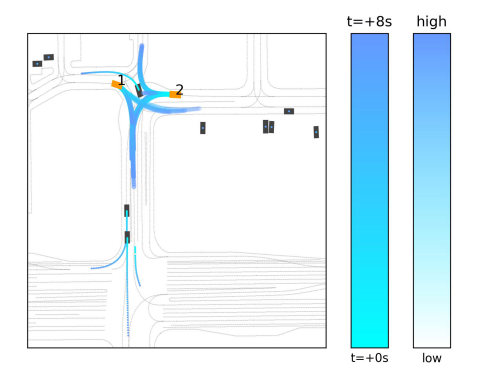
Therefore, for $\gamma=0$, our loss is equivalent to standard losses for learning a set of weighted trajectories, such as those used in [3,27,28]. However, for $\gamma>0$, our novel coverage loss \mathcal{L}_{cov} also allows the user to prioritize coverage of LNE.

IV. EXPERIMENTS

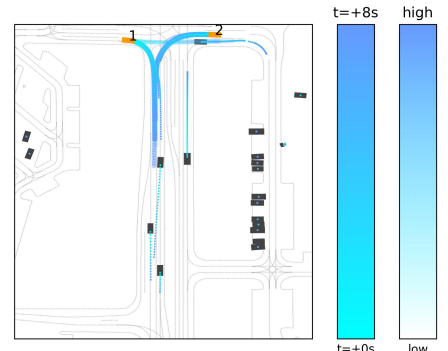
We now introduce the dataset and experiments demonstrating the effectiveness of our approach compared to several baselines.

A. Experiment Design

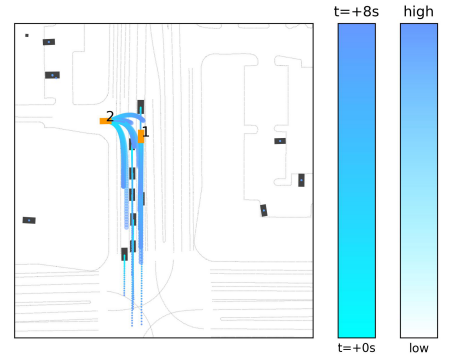
a) Dataset Description: We evaluate our model on the interactive split of the large-scale Waymo Open Motion Dataset (WOMD) [42], which has a diverse set of real-world traffic scenes. The diversity of interaction, and long prediction horizon make it especially challenging for prediction. The interactive prediction task requires the model to



(a) **Yield.** Agents 1 and 2 exhibit a multi-modal yield interaction either 1 or 2 may turn towards the lower street, causing the other to break. Other interactions are also possible, including agent 1 going straight, affecting agent 2's timing.



(b) **Follow.** Agent 2 turns left onto the lower street but must consider agent 1's intent: if agent 1 continues straight, agent 2 can turn at a high right of speed, but if agent 1 also turns, agent 2 must follow at a lower velocity.



(c) **Low-TTC.** Three plausible risk-varying choices where agent 2 turns onto a busy street: turning out immediately in close proximity to other vehicles, waiting briefly for the middle lane, or waiting patiently for traffic to clear.

Fig. 4: Bird's eye view trajectories with interactions between agents 1 and 2. NashFormer balances predictive weighting of multiple-equilibria game-theoretic interactions, resulting in better coverage of various outcomes.

	Method	minADE ↓	$minFDE \downarrow$	Miss Rate ↓	mAP ↑
Test	LSTM Baseline [42]	1.096	5.028	0.775	0.052
	HeatIRm4 [43]	1.420	3.260	0.722	0.084
	AIR ² [44]	1.317	2.714	0.623	0.096
	DenseTNT [6]	1.142	2.490	0.535	0.165
	M2I [30]	1.351	2.833	0.554	0.124
	Scene Trans. [27]	0.977	2.189	0.494	0.119
	MTR [3]	0.918	2.063	0.441	0.204
	GameFormer (J) [45]	0.916	1.937	0.441	0.137
Val	MTR [3]	0.913	2.054	0.437	0.199
	NashFormer-Base (Ours)	0.961	2.198	0.508	0.192
	NashFormer-GT (Ours)	0.978	2.238	0.495	0.182
	NashFormer-NES (Ours)	0.944	2.146	0.483	0.193
	•				

Table I: <u>Joint</u> metrics comparing game-theory-agnostic and game-theory model at 8s. Accuracy metrics are in meters.

predict the joint future of two target agents, with up to 128 total agents per scene. The dataset provides one second of trajectory history per agent, and the prediction horizon is eight seconds. There are 487k training scenes and 44k validation scenes for the interactive challenge. As metrics, we compute scene-averaged MoN average and final displacement errors (minADE, minFDE), miss rate, and mean average precsion (mAP), defined in [42].

- b) Model Implementation: For each focal agent of the target agents to predict, the state histories of all other agents and the map are first normalized to the coordinate frame of the focal agent. The transformer structure is identical to that of [3]. For the overall loss (17), we use $\alpha=1$, $\beta=1$, and $\gamma=10$. We use b=10 as the Mean Shift bandwidth parameter.
- c) Coverage evaluation: We evaluate the coverage of semantic interactions, or *semantic diversity*, by the entropy of the weights assigned to a set of (post-hoc) interaction labels q [7] on the validation set,

$$\mathcal{H}_{\mathcal{S}} = -\sum_{m=1}^{M} q_m \log q_m, \tag{18}$$

where $M:=|\mathcal{S}|$ is the total number of semantic interaction modes, $q_m:=z_m^{-1}\sum_{k=1}^K\mathbb{1}[\tau_k\in\mathcal{S}_m]w_k$ is the sum of the predictor weights assigned to interaction mode $m,\,z_m$

is a normalizing constant, and \mathcal{S}_m is the set of trajectories that satisfy a label $m \in \mathcal{S}$, such as a specific interaction category, such as "A yielding to B". In this work, we compute several semantic diversity metrics for the final samples selected by NMS: \mathcal{H}_{Util} for the cumulative advantage, \mathcal{H}_{Yield} for yield scenarios, \mathcal{H}_{Follow} for follow scenarios, \mathcal{H}_{TTC} for low-proximity maneuvers. Importantly, we do not provide the interaction labels during training or during inference. In experiments we report the dataset-averaged $H_{[\cdot]}$ as defined in (18) to gauge coverage.

B. WOMD Interactive Prediction Task

Quantitative Results. Table I details the performance of our model on the Waymo Interactive Dataset [42] against several recent [3, 43, 45] baseline models that do not use an additional coverage loss (16) as in our approach. We present scores for three models: Nashformer-Base, which does not use the additional coverage loss (16) and employs NMS sampling at a standard threshold of 2.5 meters; NashFormer-GT, which uses the game-theoretic coverage loss (16) along with NMS (also at 2.5 meters) to increase coverage of multiple equilibria; and NashFormer-NES, which uses NES sampling in addition to the coverage loss to prioritizing sampling of multiple equilibria. Against the validation set, our base model performs similarly to the successful MTR [3] model in minADE, minFDE, and mAP, with the NES model enjoying a slight boost in performance due to inference-time reasoning about gametheoretic equilibria.

Both GT and NES variants of NashFormer enjoy a lower miss rate than the base model, which supports the hyporthesis that generic predictors may emit redundant modes, even with NMS sampling, as presented in Fig. 1.

Ablation Study. Table II presents an ablation study on the effect of both the game-theoretic coverage loss (16) and sampling strategy on the coverage of local equilibria for three coverage-inducing strategies: FPS, NMS, and NES. We present the raw KL score for (16) in addition to the prediction mi-

	GT Loss	Method	Thresh.	KL↓	minADE ↓	$N_{\mathrm{modes}} \uparrow$	$\mathcal{H}_{Util.}\uparrow$	$\mathcal{H}_{Yield} \uparrow$	$\mathcal{H}_{Follow} \uparrow$	$\mathcal{H}_{TTC} \uparrow$
	Х	FPS (top 24)	-	0.302	1.370	1.512	0.182	0.035	0.018	0.018
Cama Agnostia	X	FPS (top 12)	-	0.302	1.168	1.529	0.573	0.090	0.053	0.055
Game-Agnostic	X	NMS	2.5	0.302	0.961	1.575	1.193	0.142	0.094	0.086
	X	NMS	10.0	0.301	1.166	1.546	0.700	0.142	0.073	0.072
	✓	NMS	2.5	0.104	0.984	2.069	1.362	0.162	0.120	0.120
Game-Aware	✓	NMS	10.0	0.104	1.203	2.018	1.015	0.146	0.116	0.129
Game-Aware	X	NES	10.0	0.303	0.944	1.544	1.228	0.142	0.096	0.086
	/	NES	10.0	0.103	0.978	2.150	1.374	0.162	0.121	0.129

Table II: Effect of game-aware loss \mathcal{L}_{cov} and sampling strategies versus game-agnostic methods. We compare NashFormer with and without the coverage loss (16) and additionally explore several coverage-inducing sampling strategies: FPS with the top k-weighted samples (here, k is 12 or 24), NMS with both a small (2.5m) and large (10m) threshold, and NES, presented earlier. Game-theoretic analysis improves coverage of local equilibria for all metrics.

nADE, number of prediction modes covered N_{modes} , and posthoc semantic diversity scores for four interaction categories: raw utility, yielding, following, and low-TTC (close-proximity driving). Our results show that generic sampling methods such as FPS and NMS do not automatically capture game-theoretic equilibria; only NashFormer, using knowledge of the global cost landscape, captures multiple distinct LNE. For NES, we present a game-aware variant of a generic predictor (second to last row) that only uses NES without a game-theoretic loss to capture a higher number equilirbia. We note that the lower number of modes covered N_{modes} indicates that the coverage loss (16) may result in finding new equilibria; nonetheless, semantic diversity scores are still improved using only the equilibria available to the base model. In Fig. 5, we show that NashFormer better captures LNE using fewer samples than a generic predictor using NMS.

We also performed an ablation of the effect of the coverage loss coefficient γ on the minADE and number of modes covered. The base NashFormer model using NMS at a 2.5 thresholded covered 1.546 modes with a minADE score of 0.98 (see Table 2). By varying $\gamma \in [0,100]$, the number of modes covered by NashFormer is in the range [1.55, 3.50] and sacrifices only up to in minADE, in the range [0.98, 1.07]. Compared to other approach such as FPS that naively increase pairwise distance between samples and sacrifice minADE, NashFormer prioritizes diverse *equilibria* that are intrinsically local optima in the posterior trajectory distribution.

Qualitative Results Our experimental results show that Nash-Former achieves higher coverage of scenario-specific modalities versus a baseline without game-awareness. As demonstrated in Fig. 4, NashFormer improves coverage of empirically rare scenarios on the basis of their existence as equilibria, providing insight into different possible outcomes. In Fig. 4(a), multiple yield interactions are possible, including at various timings, depending on the choices of agents 1 and 2. In Fig. 4(b), multiple follow interactions are possible between agents 1 and 2 depending on if agent 1 chooses to go forward or turn right. In Fig. 4(c), agent 2 may choose various risky behavior depending on their perceived cumulative advantage; it is important for other road agents, especially agent 1, to consider these choices or risk violating close-proximity safety protocols. While the above results hold for the WOMD interactive dataset, which has fixed interaction complexity, we

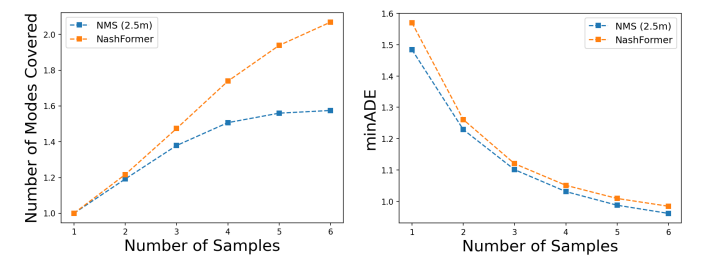


Fig. 5: Mode coverage (left) and minADE (right) as the number of prediction samples increases for the full NashFormer model versus an off-the-shelf predictor with NMS sampling at a 2.5 meter threshold. NashFormer permits each sample to contribute to coverage, while the off-the-shelf predictor plateaus around the fourth sample. Moreover, NashFormer does not suffer significant loss of minADE accuracy as it's permitting better coverage.

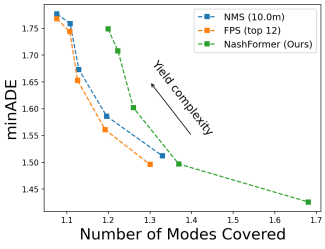


Fig. 6: Coverage versus minADE (meters) for NashFormer versus baseline models. NashFormer achieves up to 33.6 percent higher coverage of semantic modes while minADE is largely unaffected by the increased sample diversity.

show in the following section that NashFormer can better generalize to even more challenging interactive scenarios with *increasing* interaction complexity.

C. High-Complexity Yielding Scenarios

We demonstrate the efficacy of our model on several high-complexity network interactions that specifically involve yielding. These scenarios capture NashFormer's capability to cover distinct yielding outcomes when decision uncertainty is high. **Filtering for Complex Network Interactions** To evaluate coverage of game-theoretic outcomes, we augment the WOMD training set with labels indicating high-level yield interactions. Specifically, we consider two agents i and j as nodes in a directed graph G to satisfy yield (i,j) interaction if agent

i yields to agent j. We evaluate network interactions in which there occurs at least k yield interactions, for $0 \le k \le 4$.

Results Fig. 6 shows the trend in minADE as scenario complexity increases. NashFormer, which intrinsically samples diverse LNE, enjoys lower minADE versus other diverse sampling methods (FPS, NMS). We note that the number of modes covered decreases for all model as the complexity of interaction increases; empirically, as the number of nodes in a network interaction grows, so does the basin of attraction of multi-agent equilbria. In other words, fewer stable multi-agent equilibria may exist when agents interact in a spatially compact group. Nonetheless, NashFormer covers a more diverse set of modes while scoring lower minADE versus the other diversity-promoting methods, showing that the other methods have poor prioritization of LNE.

V. CONCLUSION

In this paper we introduce NashFormer, a prediction model that uses local Nash equilibria (LNE) to improve the coverage of prediction networks without presuming a specific maneuver taxonomy, and beyond what is afforded by metric trajectory coverage approaches. Our experiments reveal coverage of semantic interactions, lending insight into different modes of utility-driven decision-making. We believe our game-theoretic prediction framework opens several research avenues for more effective game-theoretic planning.

REFERENCES

- [1] T. F. Gonzalez, "Clustering to minimize the maximum intercluster distance," Theoretical computer science, vol. 38, pp. 293-306, 1985.
- H. Zhao, J. Gao, et al., "TNT: Target-driven trajectory prediction," in Conference on Robot Learning. PMLR, 2021, pp. 895-904.
- [3] S. Shi, L. Jiang, D. Dai, and B. Schiele, "Motion transformer with global intention localization and local movement refinement," arXiv preprint arXiv:2209.13508, 2022.
- [4] W. Luo, C. Park, et al., "JFP: Joint future prediction with interactive multi-agent modeling for autonomous driving," arXiv preprint arXiv:2212.08710, 2022.
- [5] S. Shi, L. Jiang, D. Dai, and B. Schiele, "MTR++: Multi-agent motion prediction with symmetric scene modeling and guided intention querying," arXiv preprint arXiv:2306.17770, 2023.
- J. Gu, C. Sun, and H. Zhao, "DenseTNT: End-to-end trajectory prediction from dense goal sets," in ICCV, 2021, pp. 15303-15312.
- [7] X. Huang, S. G. McGill, et al., "DiversityGAN: Diversity-aware vehicle motion prediction via latent semantic sampling," IEEE RA-L, vol. 5, no. 4, pp. 5089-5096, 2020.
- [8] X. Huang, G. Rosman, et al., "HYPER: Learned hybrid trajectory prediction via factored inference and adaptive sampling," in ICRA. IEEE, 2022, pp. 2906-2912.
- [9] T. Başar and G. J. Olsder, Dynamic noncooperative game theory. SIAM,
- J. F. Fisac, E. Bronstein, et al., "Hierarchical Game-Theoretic planning for autonomous vehicles," in ICRA, May 2019, pp. 9590-9596.
- [11] D. Fridovich-Keil, E. Ratner, et al., "Efficient iterative Linear-Quadratic approximations for nonlinear Multi-Player General-Sum differential games," in ICRA, May 2020, pp. 1475-1481.
- [12] M. Wang, Z. Wang, et al., "Game-theoretic planning for self-driving cars in multivehicle competitive scenarios," IEEE T-RO, vol. 37, no. 4, pp. 1313-1325, 2021.
- O. So, K. Stachowicz, and E. A. Theodorou, "Multimodal maximum entropy dynamic games," arXiv preprint arXiv:2201.12925, 2022.
- [14] P. Geiger and C.-N. Straehle, "Learning game-theoretic models of multiagent trajectories using implicit layers," in AAAI, vol. 35, no. 6, 2021, pp. 4950-4958.

- [15] S. Le Cleac'h, M. Schwager, Z. Manchester, et al., "ALGAMES: A fast solver for constrained dynamic games," in RSS, 2020.
- [16] S. Le Cleac'h, M. Schwager, and Z. Manchester, "LUCIDgames: Online unscented inverse dynamic games for adaptive trajectory prediction and planning," IEEE RA-L, vol. 6, no. 3, pp. 5485-5492, 2021.
- [17] W. Schwarting, A. Pierson, S. Karaman, and D. Rus, "Stochastic dynamic games in belief space," IEEE T-RO, vol. 37, no. 6, pp. 2157-2172, 2021.
- [18] N. Mehr, M. Wang, and M. Schwager, "Maximum-entropy multi-agent dynamic games: Forward and inverse solutions," 2021. [Online]. Available: https://arxiv.org/abs/2110.01027
- [19] W. Schwarting, A. Pierson, et al., "Social behavior for autonomous vehicles," PNAS, vol. 116, no. 50, pp. 24972-24978, 2019.
- [20] J. L. V. Espinoza, A. Liniger, et al., "Deep interactive motion prediction and planning: Playing games with motion prediction models," in L4DC. PMLR, 2022, pp. 1006-1019.
- [21] O. So, P. Drews, et al., "MPOGames: Efficient multimodal partially observable dynamic games," in ICRA. IEEE, 2023, pp. 3189-3196.
- [22] B. D. Ziebart, A. L. Maas, et al., "Maximum entropy inverse reinforcement learning." in AAAI, vol. 8, 2008, pp. 1433-1438.
- M. Wulfmeier, D. Rao, et al., "Large-scale cost function learning for path planning using deep inverse reinforcement learning," The International Journal of Robotics Research, vol. 36, no. 10, pp. 1073-1087, 2017.
- [24] T. Phan-Minh, F. Howington, et al., "Driving in real life with inverse reinforcement learning," arXiv preprint arXiv:2206.03004, 2022.
- [25] B. Evens, M. Schuurmans, and P. Patrinos, "Learning mpc for interaction-aware autonomous driving: A game-theoretic approach," in 2022 European Control Conference (ECC), 2022, pp. 34-39.
- [26] D. Helbing and P. Molnar, "Social force model for pedestrian dynamics," Physical review E, vol. 51, no. 5, p. 4282, 1995.
- [27] J. Ngiam, B. Caine, et al., "Scene transformer: A unified architecture for predicting multiple agent trajectories," in ICLR, June 2021.
- [28] B. Varadarajan, A. Hefny, et al., "MultiPath++: Efficient information fusion and trajectory aggregation for behavior prediction," Nov. 2021.
- [29] S. Kumar, Y. Gu, et al., "Interaction-based trajectory prediction over a hybrid traffic graph," in IROS. IEEE, 2021, pp. 5530-5535.
- [30] Q. Sun, X. Huang, et al., "M2I: From factored marginal trajectory prediction to interactive prediction," in CVPR, 2022, pp. 6543-6552.
- [31] Y. Ban, X. Li, et al., "Â deep concept graph network for interactionaware trajectory prediction," in ICRA. IEEE, 2022, pp. 8992-8998.
- S. Shiroshita, S. Maruyama, et al., "Behaviorally diverse traffic simulation via reinforcement learning," in IROS. IEEE, 2020, pp. 2103–2110.
- [33] T. Salzmann, B. Ivanovic, P. Chakravarty, and M. Pavone, "Trajectron++: Dynamically-feasible trajectory forecasting with heterogeneous data," in ECCV. Springer, 2020, pp. 683-700.
- [34] X. Huang, S. G. McGill, et al., "Uncertainty-aware driver trajectory prediction at urban intersections," in ICRA. IEEE, 2019, pp. 9718-9724.
- [35] T. Phan-Minh, E. C. Grigore, et al., "Covernet: Multimodal behavior prediction using trajectory sets," in *CVPR*, 2020, pp. 14 074–14 083. X. Huang, G. Rosman, *et al.*, "TIP: Task-informed motion prediction
- for intelligent vehicles," in IROS. IEEE, 2022.
- R. McAllister, B. Wulfe, et al., "Control-aware prediction objectives for autonomous driving," in ICRA, 2022.
- Z. Wang, O. So, et al., "Variational inference MPC using tsallis divergence," arXiv preprint arXiv:2104.00241, 2021.
- [39] J. Kim and I. Yang, "Maximum entropy optimal control of continuoustime dynamical systems," IEEE Transactions on Automatic Control,
- [40] Y. Cheng, "Mean shift, mode seeking, and clustering," IEEE T-PAMI, vol. 17, no. 8, pp. 790-799, 1995.
- [41] D. Comaniciu and P. Meer, "Mean shift: A robust approach toward feature space analysis," IEEE T-PAMI, vol. 24, no. 5, pp. 603-619, 2002.
- S. Ettinger, S. Cheng, et al., "Large scale interactive motion forecasting for autonomous driving: The waymo open motion dataset," in CVPR, 2021, pp. 9710-9719.
- X. Mo, Y. Xing, and C. Lv, "Heterogeneous edge-enhanced graph attention network for multi-agent trajectory prediction," In Workshop in Autonomous Driving, CVPR, 2021.
- [44] D. Wu and Y. Wu, "AIR2 for interaction prediction," arXiv preprint arXiv:2111.08184, 2021.
- [45] Z. Huang, H. Liu, and C. Lv, "Gameformer: Game-theoretic modeling and learning of transformer-based interactive prediction and planning for autonomous driving," arXiv preprint arXiv:2303.05760, 2023.